

A Computer Study of the Raman Spectra of the $(\text{GaN})_{129}$, $(\text{SiO}_2)_{86}$, and $(\text{GaN})_{54}(\text{SiO}_2)_{50}$ Nanoparticles

A. E. Galashev

Institute of Industrial Ecology, Ural Branch, Russian Academy of Sciences, Yekaterinburg, 620219 Russia

e-mail: galashev@ecko.uran.ru

Received January 21, 2011

Abstract—The Raman spectra of the $(\text{GaN})_{129}$, $(\text{SiO}_2)_{86}$, and $(\text{GaN})_{54}(\text{SiO}_2)_{50}$ nanoparticles were calculated using the molecular dynamics method. The spectrum of $(\text{SiO}_2)_{86}$ had three broad bands only, whereas the Raman spectrum of $(\text{GaN})_{129}$ contained a large number of overlapping bands. The form of the Raman spectrum of $(\text{GaN})_{54}(\text{SiO}_2)_{50}$ was determined by the arrangement of the GaN and SiO_2 components in it. The nanoparticle with a GaN nucleus had a continuous fairly smooth spectrum over the frequency range $0 \leq \omega \leq 600 \text{ cm}^{-1}$, whereas the spectrum of the nanoparticle with a SiO_2 nucleus contained well-defined bands caused by vibrations of groups of atoms of different kinds and atoms of the same kind.

Keywords: silicon dioxide, molecular dynamics, gallium nitride, nanoparticles, Raman spectra

DOI: 10.1134/S1990793112050041

INTRODUCTION

The totality of microcrystalline quartz kinds are traditionally divided into two types on the basis of crystalline habitus determined using optical microscopy [1]. Granular diversities include chert and fine-grained sandstone, whereas fibrous varieties of fine-crystalline quartz are combined under a name of chalcedonies. The \tilde{n} axis in chalcedonies is most often perpendicular to the long fiber axis. Although the majority of chalcedonies grow with just this orientation, special chalcedonies with the \tilde{n} axis parallel to fibers or directed at an angle of 30° to them are also numerous. Raman scattering is a powerful and widely used method for studying admixtures and defects in materials. This technique is used to rapidly identify materials. Because of high sensitivity of vibrational frequencies and scattering intensities to small differences in crystal structure, this method is successfully used to reveal polymorphism of materials. Raman spectroscopy cannot however be used to determine the type of vibrations (longitudinal or transverse) to which a band is related. Micro-Raman measurements over the frequency range $50 \leq \omega \leq 1250 \text{ cm}^{-1}$ revealed the presence of several intense bands characteristic of pure SiO_2 samples. The most intense peaks are situated at 129, 220, and 501 cm^{-1} [3]. Less intense bands at 250–480, 650–850, and $1040\text{--}1210 \text{ cm}^{-1}$ were, however, also observed. Asymmetric and less intense bands and also a peak at 220 cm^{-1} likely appear because of mode overlapping [4].

The presence of low-energy Raman lines localized between 95 and 250 cm^{-1} in GaN grown by molecular

beam epitaxy was for the first time observed in [5]. According to [6], these peaks are only present in the spectra of GaN and GaAs. It was reported in [7] that these peaks were also characteristic of GaN layers grown by molecular beam epitaxy on sapphire and GaAs substrates. Their intensity decreased as the temperature increased, and they completely disappeared at room temperature. They were therefore assigned to electronic excitation of donors [5]. More recent measurements in a magnetic field at a high pressure however showed that all the lines were caused by vibrational Raman scattering, and their temperature dependence was caused by a resonance process [8]. Theoretical calculations showed that these lines were related to As admixtures in GaN [9]. Semiconductors contain many electronic excitations thanks to free and bound charges. Electronic excitations can be related to lattice vibrations. The influence of free charge carriers on Raman spectra and their relation to longitudinal optical phonons was considered in [10] for the example of *N*-type GaN films.

It was shown experimentally that, because of epitaxial growth of GaN at $293\text{--}1373 \text{ K}$ brought in contact with SiO_2 , compression and shear stresses appeared close to bases of growing GaN pyramids [11]. These stresses had maximum values of 3 and 0.9 GPa , respectively. They were caused by different thermal expansion coefficients of GaN and SiO_2 . An analysis of the field of stresses using the method of finite elements allowed the geometric conditions of experiment necessary for the attainment of the required morphology characteristics of GaN crystals to be predicted and optimized.

Parameters of the Tersoff optimized potential

Element	A , eV	B , eV	λ_1 , Å ⁻¹	λ_2 , Å ⁻¹	R , Å	D , Å
Silicon	1803.79	471.195	2.62392	1.88891	2.76581	0.31772
Oxygen	3331.06	260.476	3.78336	3.34402	2.78681	0.52612
Gallium	993.88	136.123	2.50842	1.49082	3.5	0.1
Nitrogen	6368.21	511.205	5.60181	3.16170	2.08389	0.33133
Element	β	n	h	c	d	χ
Silicon	1.0999×10^{-6}	0.78766	-0.56239	1.0039×10^5	16.21701	1
Oxygen	1.00270	3.98638	-0.52909	0	1	1
Gallium	0.23586	3.47290	0.71459	0.07630	19.79647	1
Nitrogen	4.4422×10^{-3}	2.42635	-0.52909	2.2955×10^4	24.78674	1

Note: Parameter values for silicon, oxygen, and nitrogen were obtained in [14]; parameters for gallium were taken from [15].

The development of technologies for the production of optoelectronic devices and high-power devices working at a high frequency requires the size of active material blocks to be decreased even to separate nanoparticles. The structure of materials is usually determined from Bragg peaks in their diffraction patterns. Fine powders, however, do not possess extended structural coherence of usual crystals and give diffraction patterns with a well-defined diffusion component and several broad Bragg-like special features. For this reason, the traditional diffraction technique is very difficult to use for structure determination. Raman scattering from nanoparticles whose size is smaller than 5 nm has not been studied as yet. Such studies can, however, be performed using computer experiments.

The purpose of this work was to use the molecular dynamics method for obtaining the Raman spectra of the (GaN)₁₂₉, (SiO₂)₈₆, and (GaN)₅₄(SiO₂)₅₀ nanoparticles. The (GaN)₅₄(SiO₂)₅₀ nanoparticle was represented by species of two types: a GaN particle covered by a SiO₂ layer and a SiO₂ particle with a GaN layer deposited on it.

COMPUTER MODEL

The Tersoff potential extensively used in simulation of atomic semiconducting systems is an empirical function determined by two-particle interactions, which depend on local environment.

The potential energy of the system U is written as

$$U = \sum_i U_i = \frac{1}{2} \sum_{i \neq j} \Phi_{ij},$$

$$\Phi_{ij} = f_c(r_{ij}) [f_r(r_{ij}) + b_{ij} f_a(r_{ij})],$$

$$f_r(r_{ij}) = A_{ij} \exp(-\lambda_{ij}^{(1)} r_{ij}),$$

$$f_a(r_{ij}) = B_{ij} \exp(-\lambda_{ij}^{(2)} r_{ij}),$$

$$f_c(r_{ij}) = \begin{cases} 1, & r_{ij} < R_{ij}, \\ \frac{1}{2} - \frac{1}{2} \cos\left(\pi \frac{r_{ij} - R_{ij}}{S_{ij} - R_{ij}}\right), & R_{ij} < r_{ij} < S_{ij}, \\ 0, & r > S_{ij}, \end{cases} \quad (1)$$

$$b_{ij} = \chi_{ij} (1 + \beta_i \zeta_{ij}^{n_i})^{-1/(2n_i)}, \quad (1)$$

$$\zeta_{ij} = \sum_{k \neq i, j} f_c(r_{ik}) \omega_{ik} g(\theta_{ijk}), \quad (2)$$

$$g(\theta_{ijk}) = 1 + \frac{c_i^2}{d_i^2} - \frac{c_i^2}{\left[d_i^2 + (h_i - \cos \theta_{ijk})^2\right]},$$

$$\lambda_{ij}^{(k)} = (\lambda_i^{(k)} + \lambda_j^{(k)})/2; \quad A_{ij} = (A_i A_j)^{1/2}; \quad B_{ij} = (B_i B_j)^{1/2}; \quad (3)$$

$$R_{ij} = (R_i R_j)^{1/2}; \quad S_{ij}^{(2)} = (S_i S_j)^{1/2},$$

where the “ i ,” “ j ,” and “ k ” indices determine atoms, r_{ij} is the bond length between atoms i and j , and θ_{ijk} is the angle between the ij - and ik -bonds. The χ_{ij} parameter in (1) is used to reduce the strength of heteropolar bonds. Here, $\chi_{ii} = 1$ and $\chi_{ij} = \chi_{ji}$, and only one independent parameter is therefore necessary to describe a pair of atomic types. The ω_{ik} parameter in (2) can vary substantially when different types of atoms are considered, but it is mostly assumed that $\omega_{ik} = 1$. The $\lambda_{ij}^{(k)}$, A_{ij} , B_{ij} , R_{ij} , and S_{ij} potential parameters describing interaction between atoms of kinds i and j were calculated using arithmetical and geometrical means (Eq. (3)). The procedure for fitting the other parameters when the original Tersoff potential [12] is used is described in [13].

The Tersoff potential parameters for silicon, oxygen, gallium, and nitrogen are listed in the table [14, 15]. Potentials for Si, O, and N contain optimized parameters. The procedure selected for the optimization of potential parameters involved simultaneous fitting of energy and forces to the values obtained in calculations by the density functional theory method

rather than the use of traditional potential fitting to physical properties [14].

The initial configurations of nanoparticles were created by cutting spheres and spherical layers from the GaN crystal with the wurtzite structure and the α -quartz crystal. In GaN and SiO₂ spheres, the necessary stoichiometry was retained. When nanoparticles containing both GaN and SiO₂ were created, a sphere with either of these components was surrounded by a spherical layer of the other component. The preliminarily constructed GaN crystal had the following lattice parameters: a , $b = 0.3181$ nm and $c = 0.5184$ nm [16]. Packing of SiO₄ tetrahedra for obtaining an α -quartz crystal with the parameters a , $b = 0.5082$ nm and $c = 0.55278$ nm [17] was obtained using the GRINSP program for the generation of inorganic crystal structures [18]. To prepare a nanoparticle with a GaN nucleus, a sphere formed by GaN was put into a spherical SiO₂ layer with providing coincidence of their centers. The preparation of nanoparticles with a SiO₂ nucleus included similar addition of a sphere formed by SiO₂ to a GaN spherical layer. In both cases, spherical layer atoms situated at a distance smaller than some selected r_m value from any sphere atom were removed from the region including the surface of the sphere and the lower spherical layer boundary. As a result, after assembly of nanoparticles, we obtained the following minimum distances between atoms of different kinds: 3.23 (Ga–Si), 2.67 (Ga–O), 2.22 (N–Si), and 2.00 (N–O). The size of a sphere was sufficient for the accommodation of 50 SiO₂ structural units or 54 GaN atomic units. The environment contained a similar number of structural units of each type. Atoms farthest from the center of mass of the created nanoparticle were removed. Calculations of physical properties were performed using a classic molecular dynamics ensemble, which was a particular case of a microcanonical ensemble. Equations of motion were integrated following the fourth-order Runge–Kutta method with a $\Delta t = 10^{-16}$ s time step. At the preliminary stage of calculations 100000 Δt long, atom velocities were corrected to balance system at a 300 K temperature. The main stage of calculations was performed without any corrections; it was 1000000 time steps long. As a result, the following temperatures were obtained for nanoparticles: 303.2 ((SiO₂)₈₆), 314.5 ((GaN)₁₂₉), 303.3 ((GaN)₅₄(SiO₂)₅₀ with a SiO₂ nucleus), and 304.5 K ((GaN)₅₄(SiO₂)₅₀ with a GaN nucleus).

RAMAN SPECTRA

The Raman spectra of clusters can be calculated via the autocorrelation function of polarizability fluctuations. Each atom in a model can be treated as a polarizable point dipole situated in the nucleus of the atom. As a result of interactions with neighboring atoms, induced dipole moment \mathbf{d}_i and polarizability \mathbf{a}_i are created in an atom with permanent polarizability $\mathbf{a}_{i,0}$ [19],

$$\mathbf{d}_i = \mathbf{d}_{i,0} + \mathbf{a}_{i,0} \sum_{j \neq i} \mathbf{T}_{ij} \mathbf{d}_j,$$

$$\mathbf{a}_i = \mathbf{a}_{i,0} + \mathbf{a}_{i,0} \sum_{j \neq i} \mathbf{T}_{ij} \mathbf{a}_j.$$

Here, \mathbf{T}_{ij} is the dipole-dipole interaction tensor,

$$\mathbf{T}_{ij} = \frac{1}{|r_{ij}|^3} (3\hat{\mathbf{r}}_{ij}\hat{\mathbf{r}}_{ij} - \mathbf{1}). \quad (4)$$

In (4), $\hat{\mathbf{r}}_{ij}$ is the unit vector in the $\mathbf{r}_i - \mathbf{r}_j$ direction, where \mathbf{r}_i and \mathbf{r}_j are the positions of the nuclei of atoms i and j , and $\mathbf{1}$ denotes a unit 3×3 tensor. We used the following atomic polarizability values: 3.75 (Si), 0.793 (O), 8.1 (Ga), and 1.1 \AA^3 (N). The electric charges were (in elementary electric charge units) 4 (Si), -2 (O), 3 (Ga), and -3 (N) [20]. The standard iteration procedure [21] was used at each time step to calculate induced dipole moments \mathbf{d}_i . The accuracy of \mathbf{d}_i calculations was $10^{-5} - 10^{-4}$ D.

The static dielectric constant ϵ_0 was calculated from total dipole moment \mathbf{d} fluctuations [22],

$$\epsilon_0 = 1 + \frac{4\pi}{3VkT} \left[\langle \mathbf{d}^2 \rangle - \langle \mathbf{d} \rangle^2 \right],$$

where V is the nanoparticle volume and k is the Boltzmann constant.

Permittivity $\epsilon(\omega)$ as a function of frequency ω was represented by the $\epsilon(\omega) = \epsilon'(\omega) - i\epsilon''(\omega)$ complex value, which was determined using the equation [22, 23]

$$\frac{\epsilon(\omega) - 1}{\epsilon_0 - 1} = - \int_0^{\infty} \exp(-i\omega t) \frac{dF}{dt} dt = 1 - i\omega \int_0^{\infty} \exp(-i\omega t) F(t) dt,$$

where the $F(t)$ function is the normalized autocorrelation function of the total dipole moment of a nanoparticle,

$$F(t) = \frac{\langle \mathbf{d}(t)\mathbf{d}(0) \rangle}{\langle \mathbf{d}^2 \rangle}.$$

The $J(\omega)$ Raman spectrum excited by not polarized light is given by the equation [19] (if $\omega < 0$, we have Stokes and, if $\omega > 0$, anti-Stokes spectrum lines)

$$J(\omega) = \frac{\omega}{(\omega_L - \omega)^4} \left[1 - \exp\left(-\frac{\hbar\omega}{kT}\right) \right] \times \text{Re} \int_0^{\infty} dt e^{i\omega t} \langle \Pi_{xz}(t)\Pi_{xz}(0) \rangle,$$

where

$$\Pi(t) \equiv \sum_{j=1}^N [\mathbf{a}_j(t) - \langle \mathbf{a}_j \rangle],$$

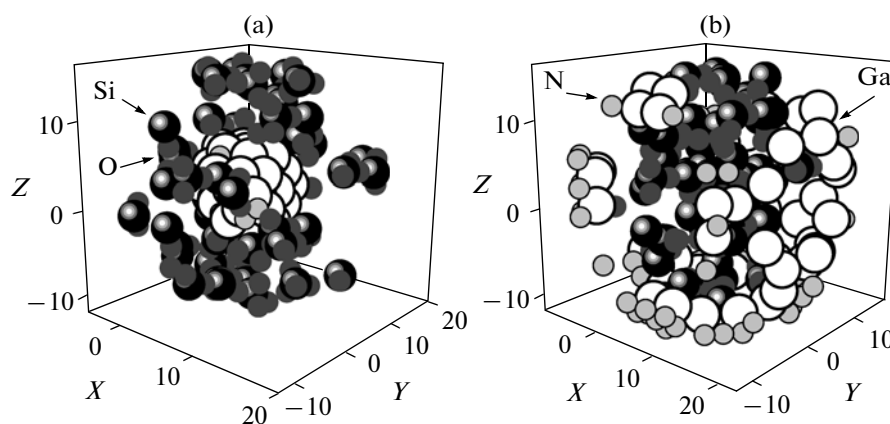


Fig. 1. Configurations of $(\text{GaN})_{54}(\text{SiO}_2)_{50}$ nanoparticles corresponding to time 100 ps; nanoparticle nucleus is (a) GaN and (b) SiO_2 .

ω_L is the exciting laser frequency, Π_{xz} is the xz component of the $\Pi(t)$ value, the x axis is directed along the bisectrix of the O–Si–O angle of the SiO_2 structural unit or along the Ga–N bond determining the induced dipole direction. Simulation was performed using $\omega_L = 194363 \text{ cm}^{-1}$ (argon laser green line, $\lambda = 514.5 \text{ nm}$).

CALCULATION RESULTS

Bond energies in $(\text{SiO}_2)_{86}$ and $(\text{GaN})_{129}$ particles calculated in this work were -9.6 and -4.7 eV/atom , respectively. The corresponding experimental values for α -quartz and gallium nitride with the wurtzite structure are -9.058 [24] and -4.529 [25]. The configurations of nanoparticles containing both SiO_2 and GaN and obtained at time 100 ps are shown in Fig. 1. Packing of SiO_2 , especially when these structural units

are arranged externally in a nanoparticle, is closer to the amorphous state rather than α -quartz. In both cases, separate oxygen atoms become detached from Si atoms and closely approach Ga atoms. If GaN is situated in the central part of a nanoparticle, the surface layer consisting of SiO_2 is strongly inhomogeneous and contains breaks. The GaN nucleus remains sphere-shaped during whole calculations. The N and Ga atoms are strongly bound with each other. During calculations, these bonds remain intact, but N atoms shift inside the GaN nucleus, and Ga atoms, outside it. If GaN is situated on the surface of a cluster, N atoms closely approach Ga atoms and do not penetrate inside the cluster. Ga atoms can be in contact with both Si and O atoms. Except loss of separate O atoms, the framework of SiO_2 is retained. The inside SiO_2 nucleus has dense and loose regions. Ga atoms fairly closely approach this nucleus.

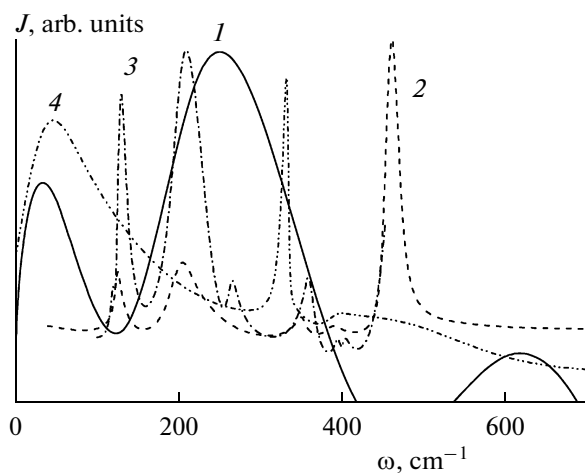


Fig. 2. Raman spectra of (1) $(\text{SiO}_2)_{86}$ nanoparticle, (2) α -quartz, (3) natural chalcedony from Arizona [26], and (4) SiO_2 film grown on sapphire [27].

The Raman spectra of the $(\text{SiO}_2)_{86}$ (α -quartz) nanoparticle, natural chalcedony from Arizona [26], and a SiO_2 film [27] grown on sapphire are shown in Fig. 2. The spectra of crystalline quartz were measured at $297 \pm 3 \text{ K}$. The low-frequency region with $\omega < 50 \text{ cm}^{-1}$ was not considered in [27] because, according to the authors, strong spurious scattering was observed at these frequencies. The strongest bands of crystalline SiO_2 were situated at 128 , 206 , and 464 cm^{-1} . In addition, two bands at 696 and 808 cm^{-1} were observed. The strongest band situated at 400 – 530 cm^{-1} corresponds to Si–O–Si symmetrical stretching-bending modes. The bands at 128 and 206 cm^{-1} correspond to torsional and O–Si–O bending modes. Recent measurements of Raman scattering from a silicon dioxide cell showed the presence of bands at 495.8 and 748.5 cm^{-1} [28]. The bands at 128 and 206 cm^{-1} are strongest in the Raman spectrum of chalcedony. Weak peaks of the same origin were observed in the J spectrum of chalcedony at 262 and 355 cm^{-1} . The SiO_2 film at $T = 293 \text{ K}$ consisted of the amorphous phase, but crystalline fragments were also present. The struc-

ture of SiO_2 glass is an amorphous network of Si atoms tetrahedrally surrounded by O atoms. Tetrahedra are linked with each other through oxygen atoms, and Si–O–Si bridges with interbond angles close to 150° are formed. In other words, each Si atom in the amorphous network is surrounded by four O atoms, and, in turn, each oxygen atom is linked with two silicon atoms. The Raman spectrum of a SiO_2 film grown on a sapphire substrate is shown in Fig. 2, curve 4. A broad band at about 400 cm^{-1} corresponds to Si–O tetrahedron rocking vibrations. A peak at 800 cm^{-1} was also observed. This peak was related to periodic bends of chemical bonds in Si–O–Si bridges. According to [27], an intense narrow peak at 378 cm^{-1} corresponds to plasma radiation in an Ar laser gas discharge tube. The stoichiometry of SiO_2 is disturbed at elevated temperatures. Nonstoichiometric SiO_2 films were obtained after annealing at 773 K for 15 min. The Raman spectrum of such a film had a broad band centered at approximately 490 cm^{-1} which corresponded to Si–Si bond vibrations. This means that amorphous silicon clusters formed in the film. The first peak in the J spectrum of a low-temperature film situated at $\sim 50\text{ cm}^{-1}$ was a wing of the Raleigh line. A well-defined low-frequency peak at 34 cm^{-1} was also observed in the Raman spectrum of the $(\text{SiO}_2)_{86}$ nanoparticle. Its appearance can also be related to the presence of Raleigh scattering. The most intense broad band appears in the vicinity of a 248 cm^{-1} frequency. This band is caused by torsional vibrations and O–Si–O bending modes. As distinct from crystalline SiO_2 , a large number of vibrations close in energy is observed in the $(\text{SiO}_2)_{86}$ nanoparticle in the vicinity of the 248 cm^{-1} band. Their superposition forms a broad intense Raman spectrum band. A weak burst in the J spectrum of the nanoparticle is also observed close to the 620 cm^{-1} frequency. This burst is an overtone of modes responsible for the intense Raman spectrum band at 248 cm^{-1} . The positions of the main Raman spectrum bands of the $(\text{SiO}_2)_{86}$ nanoparticle, α -quartz, and SiO_2 film are limited by the frequency range $0 \leq \omega \leq 500\text{ cm}^{-1}$. Two new Raman lines at 295 and 380 cm^{-1} and a weak mode at 605 cm^{-1} were recently observed in the Raman spectrum of amorphous silicon dioxide [29]. The authors relate the origin of the new branches to vibrations in five- and more-membered SiO_2 rings.

Because of thermal instability of gallium nitride crystals, GaN semiconductors are mainly produced and used in the form of thin films. The Raman spectrum of a GaN film grown on a sapphire substrate and the calculated J spectrum of the $(\text{GaN})_{129}$ nanoparticle are shown in Fig. 3. The spectrum of a GaN film has a noticeable peak at 247 cm^{-1} [30]. In [8], the origin of this peak was related to As impurities in GaN films. This mode is present at 293 K and does not disappear up to 500 K . This is the temperature at which the beginning of the electronic transition with an increase in the number of donors is expected. The

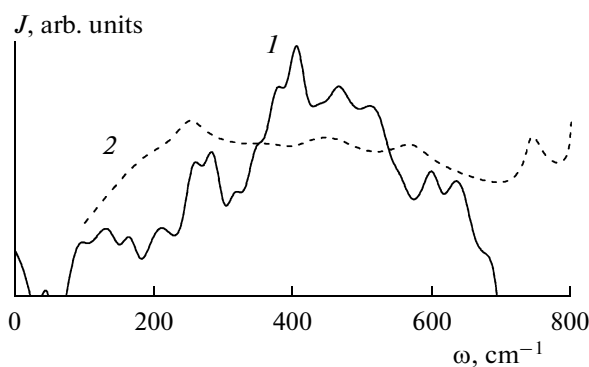


Fig. 3. Raman spectra of (1) $(\text{GaN})_{129}$ nanoparticle and (2) GaN film grown on a sapphire substrate [30].

peak at 558 cm^{-1} , which appears in the Raman spectrum, corresponds to the existence of stresses in GaN films with the wurtzite structure. The E_2 additional active Raman mode is responsible for the appearance of this peak. When stresses appear, the peak shifts toward higher frequencies; its localization at 566 cm^{-1} was mentioned. The longitudinal asymmetric vibration mode is observed at 733 cm^{-1} . This mode has an obvious “tail” extended toward high frequencies. It is present in the form of a prominent signal at low temperatures. The coalescing lines at 410 and 420 cm^{-1} are acoustic overtones [30]. The lines at 417 and 750 cm^{-1} related to sapphire were excluded from the spectrum. The Raman spectrum of the $(\text{GaN})_{129}$ nanoparticle is continuous and contains several bands localized at $0 \leq \omega \leq 650\text{ cm}^{-1}$. The calculated Raman spectrum of the $(\text{GaN})_{129}$ nanoparticle has a noticeable peak of bosons (at 131 cm^{-1}) and two accompanying subpeaks at 98 and 164 cm^{-1} (Fig. 3). The boson peak is a universal special feature of the Raman spectra of most of glasses. This peak is equally strong in many glasses and weakly changes as glass connectedness decreases. This observation was used in [31] to draw the conclusion that the boson peak appeared because of vibrations local in character. These vibrations can be represented by a harmonic oscillator. On the whole, the form of the spectrum of the nanoparticle corresponds to the form of the spectrum of a GaN film over the frequency range $100 \leq \omega \leq 650\text{ cm}^{-1}$. The Raman spectrum of the film has a smoother relief. The mean frequency value of nanoparticle spectrum peaks at 210 , 260 , and 283 cm^{-1} is 251 cm^{-1} , which closely agrees with the position of the Raman peak observed in a GaN film (247 cm^{-1}). The most intense band in the J spectrum of the nanoparticle at 408 cm^{-1} can be treated as an acoustic overtone. Taking anharmonicity into account, the peaks at 464 , 510 , 599 , and 635 cm^{-1} can be assigned to overtones of modes with a 251 cm^{-1} mean frequency. The continuous spectrum of the $(\text{GaN})_{129}$ nanoparticle extends to $\sim 694\text{ cm}^{-1}$, whereas the J spectrum of the $(\text{SiO}_2)_{86}$ nanoparticle extends to a 415 cm^{-1} frequency only; at 415 cm^{-1} , a break of the

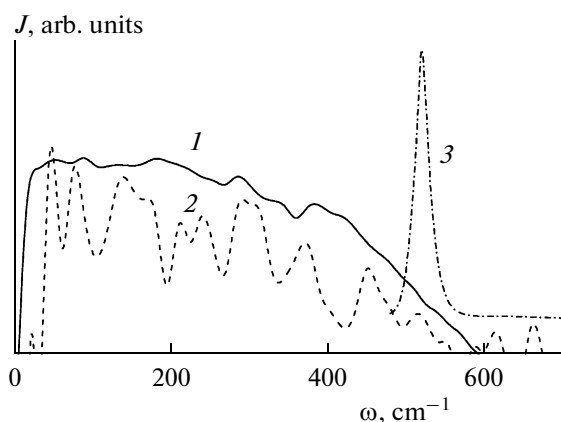


Fig. 4. Raman spectra of $(\text{GaN})_{54}(\text{SiO}_2)_{50}$ nanoparticles with (1) GaN and (2) SiO_2 nuclei and (3) Raman spectrum of GaN/ SiO_2 /Si nanocrystals with a mean size of $h = 50$ nm [32].

spectrum is observed. A large number of active frequencies in the Raman spectrum of the $(\text{GaN})_{129}$ nanoparticle is caused by its small size and a small time interval during which observations were made.

The $(\text{GaN})_{54}(\text{SiO}_2)_{50}$ nanoparticle with a GaN nucleus has a fairly smooth continuous Raman spectrum over the frequency range $0 \leq \omega \leq 600$ cm^{-1} (Fig. 4). The band in the vicinity of a 400 cm^{-1} frequency is not most intense, as with the $(\text{GaN})_{129}$ nanoparticle. The band situated close to a 204 cm^{-1} frequency is most intense. The intensity of the J spectrum linearly decreases as the frequency increases from 425 to 600 cm^{-1} . The Raman spectrum of the $(\text{GaN})_{54}(\text{SiO}_2)_{50}$ nanoparticle with a SiO_2 nucleus is characterized by a substantially cut relief. This spectrum has a somewhat higher extension compared with the J spectrum of the $(\text{GaN})_{54}(\text{SiO}_2)_{50}$ particle with a GaN nucleus. At $\omega > 559$ cm^{-1} , the Raman spectrum of the particle with a SiO_2 nucleus is not continuous. Over the frequency range $0 \leq \omega \leq 700$ cm^{-1} , the J spectrum of this particle has 11 bands. Some of these peaks (3–5) are split. The fourth peak has two subpeaks, and the third and fifth peaks have subpeaks and shoulders on the right. The first two peaks at 47 and 79 cm^{-1} should be treated as boson peaks. The position of a broad peak at 139 cm^{-1} is in agreement with the low-frequency additional active Raman mode $E_2 = 144$ cm^{-1} experimentally observed in GaN films [8]. The bands at 212 , 241 , and 291 cm^{-1} , which have the mean frequency value 248 cm^{-1} , on the one hand, correspond to the main mode (248 cm^{-1}) of the Raman spectrum of the $(\text{SiO}_2)_{86}$ nanoparticle and, on the other hand, are close to modes with the mean frequency 251 cm^{-1} observed in the J spectrum of the $(\text{GaN})_{129}$ nanoparticle. The band at 291 cm^{-1} is also close to a 295 cm^{-1} frequency mode in amorphous silicon [29]. In exactly the same way, the bands at 452 and 516 cm^{-1} correspond to 464 and 510 cm^{-1} modes in the spectrum of the $(\text{GaN})_{129}$ nanoparticle. In addition, the position of the band at

516 cm^{-1} coincides with the localization of the Raman spectrum band for a GaN nanocrystal with size 50 nm grown on a SiO_2 substrate [32]. The Raman spectrum of this nanocrystal contains only one peak (516 cm^{-1}) caused by Si atom vibrations. The position of a well-defined peak at 372 cm^{-1} is close to that of a sharp Raman spectrum peak of a SiO_2 film (378 cm^{-1}) [27] and amorphous SiO_2 (380 cm^{-1}) [29]. The other peaks at 615 and 664 cm^{-1} appear because of splitting of the peak at 620 cm^{-1} in the Raman spectrum of the $(\text{SiO}_2)_{86}$ nanoparticle. A peak close in its position (605 cm^{-1}) is also observed in amorphous SiO_2 [29]. It follows that the positions of peaks in the J spectrum of the $(\text{GaN})_{54}(\text{SiO}_2)_{50}$ nanoparticle with a SiO_2 nucleus are caused not only by collective vibrations in the GaN subsystem but also by group vibrations in the SiO_2 subsystem.

CONCLUSIONS

The calculation results show that, over the larger part of the $0 \leq \omega \leq 700$ cm^{-1} frequency range, the Raman spectra of nanoparticles consisting of SiO_2 and GaN are continuous. The Raman spectrum of the $(\text{SiO}_2)_{86}$ nanoparticle is smooth and contains a wing of Rayleigh scattering. Over the frequency range 420 – 530 cm^{-1} , a break of the spectrum is observed. Over the frequency range covered, the Raman spectrum of the $(\text{SiO}_2)_{86}$ nanoparticle is closer to the J spectrum of a SiO_2 amorphous-crystalline film than to the corresponding spectrum of crystalline or microcrystalline SiO_2 . Broad Raman spectrum bands of the $(\text{SiO}_2)_{86}$ nanoparticle are formed because of overlapping of vibrational bands close in energy. The $(\text{GaN})_{129}$ nanoparticle also has a continuous Raman spectrum. However, as distinct from the J spectrum of the $(\text{SiO}_2)_{86}$ nanoparticle, the Raman spectrum of the $(\text{GaN})_{129}$ nanoparticle has a large number of well defined bands. Over the frequency range $100 \leq \omega \leq 700$ cm^{-1} , the J spectrum of a GaN film with the wurtzite structure on the whole fits in with the Raman spectrum of the $(\text{GaN})_{129}$ nanoparticle. The form of the Raman spectrum of the $(\text{GaN})_{54}(\text{SiO}_2)_{50}$ nanoparticle depends to a substantial extent on the arrangement of components in the volume of this nanoparticle. If GaN forms its nucleus, the J spectrum has a smooth shape, and if SiO_2 occupies its center, the Raman spectrum has a large number of bands. These bands correspond to vibration of groups of atoms of different kinds and atoms of the same kind. The Raman spectrum of the nanoparticle with a SiO_2 nucleus has a larger extension, but its “tail” is not a continuous spectrum continuation.

ACKNOWLEDGMENTS

This work was supported by the Presidiums of the Ural and Far East branches of the Russian Academy of Sciences, integration project no. 09-S-2-1004.

REFERENCES

1. C. Klein and C. S. Hurlbut, Jr., *Manual of Mineralogy*, 20th ed. (Wiley, New York, 1985).
2. R. L. Folk and J. S. Pittman, *J. Sediment. Petrol.* **41**, 1045 (1971).
3. P. F. McMillan and A. C. Hess, *Phys. Chem. Minerals* **17**, 97 (1990).
4. A. Jayaraman, D. L. Wood, and R. G. Maines, Sr., *Phys. Rev. B* **35**, 8316 (1987).
5. M. Ramsteiner, J. Menniger, O. Brandt, et al., *Appl. Phys. Lett.* **69**, 1276 (1996).
6. H. Siegle, I. Loa, P. Thurian, et al., *Appl. Phys. Lett.* **70**, 909 (1997).
7. D.-S. Jiang, M. Ramsteiner, K.-H. Ploog, et al., *Appl. Phys. Lett.* **72**, 365 (1998).
8. H. Siegle, A. Kaschner, A. Hoffmann, et al., *Phys. Rev. B* **58**, 13619 (1998).
9. G. Kaczmarczyk, A. Kaschner, A. Hoffmann, et al., *Phys. Rev. B* **61**, 5353 (2000).
10. T. Kozawa, T. Kachi, H. Kano, et al., *J. Appl. Phys.* **75**, 1098 (1994).
11. T. S. Zheleva, W. M. Ashmawi, O.-H. Nam, et al., *Appl. Phys. Lett.* **74**, 2492 (1999).
12. J. Tersoff, *Phys. Rev. Lett.* **56**, 632 (1986).
13. A. Yasukawa, *Jpn. Soc. Mech. Eng.* **39**, 313 (1996).
14. S. R. Billeter, A. Curioni, D. Fischer, et al., *Phys. Rev. B* **73**, 155329 (2006).
15. Y. Nishidate and G. P. Nikishkov, *Comp. Model. Eng. Sci.* **26**, 91 (2008).
16. V. Petkov, M. Gateshki, J. Choi, et al., *J. Mater. Chem.* **15**, 4654 (2005).
17. S. Munetoh, T. Motooka, K. Moriguchi, et al., *Comp. Mater. Sci.* **39**, 334 (2007).
18. A. Le Bail, *J. Appl. Crystallogr.* **38**, 389 (2005).
19. W. B. Bosma, L. E. Fried, and S. Mukamel, *J. Chem. Phys.* **98**, 4413 (1993).
20. *Manual for Chemists*, Vol. 1, Ed. by B. P. Nikol'skii (Khimiya, Leningrad, 1971) [in Russian].
21. L. X. Dang and T.-M. Chang, *J. Chem. Phys.* **106**, 8149 (1997).
22. F. Bresme, *J. Chem. Phys.* **115**, 7564 (2001).
23. M. Neumann, *J. Chem. Phys.* **82**, 5663 (1985).
24. C. Stampfl and C. van de Walle, *Phys. Rev. B* **59**, 5521 (1999).
25. J. Serrano, A. Rubio, E. Hernandez, et al., *Phys. Rev. B* **62**, 16612 (2000).
26. K. J. Kingma and R. J. Hemley, *Am. Mineralog.* **79**, 269 (1994).
27. L. I. Berezinsky, V. P. Maslov, V. V. Tetyorkin, et al., *Semicond. Phys. Quantum Electron. Optoelectron.* **8**, 37 (2005).
28. N. Schonbachler and W. Luthy, *Measurements of Raman Lines in Silica, Dimethyl-Methylphosphonate and Methyl Salicylate* (Univ. of Bern Press, Bern, 2010). <http://www.iap.unibe.ch/publications/download/3384/en/>
29. M. Chligui, G. Guimbretiere, A. Canizares, et al., *Phys. Rev. B* (2010, in press). <http://hal.archives-ouvertes.fr/hal-00520823/en/>
30. R.-M. Wang, G.-D. Chen, J.-Y. Lin, et al., *Front. Phys. Chin.* **1**, 112 (2006).
31. J. Toulouse and P. Tick, *J. Non-Cryst. Solids* **222**, 335 (1997).
32. V. N. Bessolov, Yu. V. Zhilyaev, E. V. Konenkova, et al., *Semiconductors* **37**, 940 (2003).